Novel multiparametric bulk and single EV pipeline for adipose cell-specific biomarker discovery in paired human biospecimens

Paola Loreto Palacio[1], Jacelyn Greenwald[2], Kim Truc Nguyen[3], Dharti Shantaram[4], Bradley L. Butsch[1], Yonseok Kim[2], Mangesh Hade Dattu[1], Sabrena Noria[5], Stacy A. Brethauer[5], Bradley J. Needleman[5], Vicky Wysocki[2], Willa Hsueh[4], Eduardo Reátegui[3], Setty M. Magaña[1]*

[1]Department of Pediatrics, Center for Clinical and Translational Research, Nationwide Children's Hospital, Columbus, Ohio.

[2]Department of Chemistry and Biochemistry, The Ohio State University, Columbus, Ohio.

[3]Department of Chemical and Biomedical Engineering, The Ohio State University, Columbus, Ohio.

[4]Diabetes and Metabolism Research Center, The Ohio State University, Columbus, Ohio.

[5]Center for Minimally Invasive Surgery, Department of Surgery, The Ohio State University College of Medicine, Columbus, Ohio.

Running Title: Human adipose extracellular vesicles

***Corresponding Author:** Setty Magaña, MD, PhD

Address: Nationwide Children's Hospital
Department of Pediatrics, Division of Neurology
700 Children's Drive
Columbus, OH 43205

Telephone: 614-722-4625

Fax: 614-722-4633

Email: Setty.Magana@nationwidechildrens.org

Abstract

Obesity is a global health crisis that contributes to morbidity and mortality worldwide. Obesity's comorbid association with a variety of diseases, from metabolic syndrome to neurodegenerative disease, underscores the critical need to better understand the pathobiology of obesity. Adipose tissue, once seen as an inert storage depot, is now recognized as an active endocrine organ, regulating metabolic and systemic homeostasis. Recent studies spotlight the theranostic utility of extracellular vesicles (EVs) as novel biomarkers and drivers of disease, including obesity-related complications. Adipose-derived EVs (ADEVs) have garnered increased interest for their roles in diverse diseases, however robust isolation and characterization protocols for human, cell-specific EV subsets are limited. Herein, we directly address this technical challenge by establishing a multiparametric analysis framework that leverages bulk and single EV characterization, mRNA phenotyping and proteomics of human ADEVs directly from paired visceral adipose tissue, cultured mature adipocyte conditioned media, and plasma from obese subjects undergoing bariatric surgery. Importantly, rigorous EV phenotyping at the tissue and cell-specific level identified top 'adipose liquid biopsy' candidates that were validated in circulating plasma EVs from the same patient. In summary, our study paves the way toward a tissue and cell-specific, multiparametric framework for studying tissue and circulating adipose EVs in obesity-driven disease.

Introduction

Obesity has emerged as a global health crisis, reaching epidemic proportions and posing significant challenges to public health systems worldwide[1]. Obesity is associated with numerous metabolic disorders, as well as cancer, autoimmunity, and neurodegenerative diseases[2-6]. Adipose tissue, once considered an inert energy storage depot, is now recognized as an active endocrine organ that plays a crucial role in metabolic homeostasis and overall health[7]. Adipose tissue dysfunction, characterized by altered adipokine secretion, chronic inflammation, and impaired adipocyte differentiation, is a hallmark of obesity and a pivotal contributor to the development of obesity-related comorbidities[8,9].

Recent studies have revealed that obesity is also associated with enhanced production of adipose-derived extracellular vesicles (ADEVs)[10,11] . Extracellular vesicles (EVs) are small, membrane-bound vesicles released by cells into the extracellular space and represent a novel method of intercellular communication[12]. ADEVs and other EVs have emerged as potential players in the pathogenesis of obesity and its associated metabolic complications[13-15]. EVs harbor and transmit bioactive cargo (i.e., proteins, lipids, nucleic acids) to recipient cells, causing phenotypic and genotypic changes[16,17]. This ability has positioned EVs as central orchestrators of various processes, including normal cellular biology, immune regulation, tissue repair, and disease progression[12,18,19].

Two subsets of ADEVs include adipose tissue-derived EVs (ATEVs) and mature adipocyte-derived EVs (aEVs)—each with unique pathobiological roles and cell-specific phenotypic repertoires. ATEVs, which consist of EVs originating from a heterogenous composite of cells such as pre-adipocytes, immune cells, and stromal support cells, reflect the complex microenvironment of adipose tissue[10,20] On the other hand, aEVs are released specifically from mature adipocytes and provide a glimpse into the molecular messages that adipocytes utilize to communicate with other cells and tissues. Furthermore, ADEVs serve as a useful biological 'reference source' in the development of an adiposity-associated EV liquid biopsy.

Despite the growing interest in EVs and ADEVs, their full translational potential is hindered by several methodological and biological challenges, including a lack in standardized, reproducible, and robust isolation and cell-specific characterization protocols[21,22]. While a handful of studies have investigated human ADEVs[11,23,24], most ADEV studies have focused on rodent models[25-27], despite recognized cross-species differences in adipose markers between

rodents and humans[28]. This cross-species variation highlights the critical need for human-based obesity EV paradigms.

To address the current methodological and biological challenges hindering the translational advancement of human ADEVs in the clinic, we established a human-based, multiparametric workflow for the isolation and characterization of ADEVs from paired biospecimens derived from bariatric surgical patients. Our objectives were to: i) establish standardized protocols for EV isolation from paired human specimens (i.e. visceral adipose tissue, cultured mature adipocyte-conditioned media, and plasma); ii) employ cutting-edge technologies to optimize single and bulk adipose EV characterization; iii) characterize the adipose EV proteome in order to inform the development of an adipose EV liquid biopsy; iv) validate the tissue and cell-specific adiposity EV signature in circulating plasma EVs from the same patient, and iv) perform in silico prediction of ADEV functional roles in order to gain insights into the biological relevance of ADEVs.

Results

Multiparametric isolation and characterization of obesity-associated EVs

Figure 1 illustrates our multiparametric pipeline for EV isolation and characterization from bariatric patient adipose tissue and paired plasma. Most human EV biomarker studies have focused on biofluids or in vitro EV sources, however technical challenges must be overcome for tissue-derived EVs in order to maintain EV integrity[29-31]. To ensure our isolation method produced intact, tissue-derived adipose EVs, we performed rigorous bulk and single EV characterization, as described below.

Bulk EV characterization of paired human adipose tissue EV (ATEV), mature adipocyte EV (aEV) and plasma EV (bEV) characteristics

Microfluidic resistive pulse sensing (MRPS) was used to examine the size distribution and particle concentration of EVs from three adipose sources (ATEV, aEV, bEV) derived from the same individual (**Fig. 2,** n = 3). MRPS is an electric sensing platform that utilizes cartridges with pre-specified upper and lower limits of detection. We were interested in studying small EVs and therefore utilized the C400 cartridge (size range 65 nm to 400 nm). MRPS revealed greater particle size distribution for ATEVs compared to pure aEVs and bEVs. Median particle diameter was 86.12 nm for ATEVs, 82.26 nm for aEVs, and 78.60 nm for bEVs. Mean particle

concentration was 1.27e+13 particles/mL for ATEVs, 4.09e+12 particles/mL for aEVs, and 4.13e+12 particles/mL for bEVs (**Fig. 2A-C**).

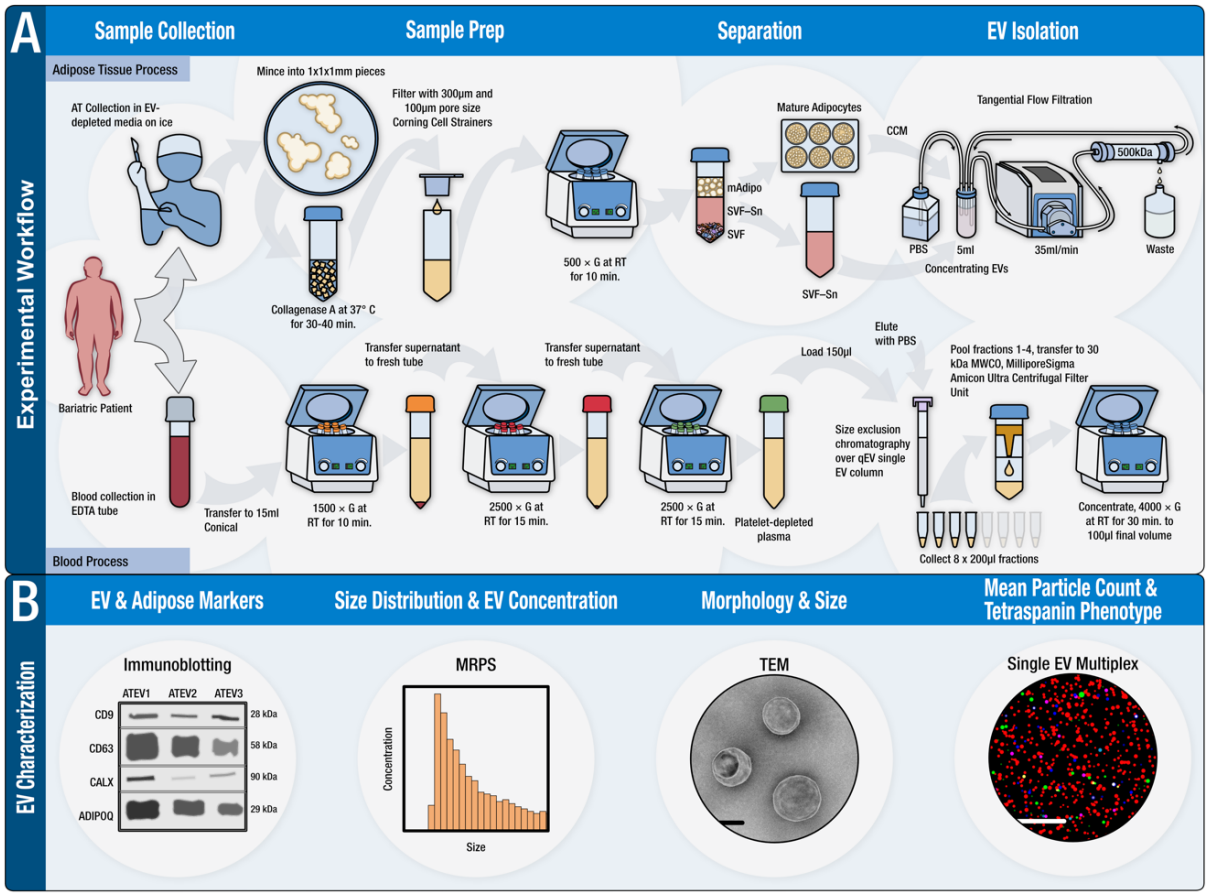

Figure 1. Workflow for EV isolation (A) and characterization (B) of ATEVs, aEVs, and bEVs. (A) Top: Visceral adipose tissue (2-10 grams) was enzymatically digested, filtered, and centrifuged, resulting in three phases: pelleted stromal vascular fraction (SVF), SVF supernatant (SVF-SN) and floating mature adipocytes. Mature adipocytes were cultured for 24 hours (see Methods), and the cell-conditioned media (CMM) was removed for EV isolation (designated aEVs) via tangential flow filtration (TFF). SVF-SN was also collected for ATEV isolation via TFF. Lower: Paired plasma was collected in EDTA tubes and subjected to centrifugation for separation of plasma and cellular components. To avoid contamination from platelet EVs, platelet depletion was performed before EV isolation using size exclusion chromatography. Fractions 1-4 were pooled and concentrated. **(B)** Multiparametric characterization of EVs by immunoblotting, microfluidic resistive pulse sensing (MRPS), transmission electron microscopy (TEM), and single EV multiplex analysis.

TEM imaging showed heterogenous particle populations, including small EVs with classic 'cup-shaped' fixation artefacts (**Fig. 2D-F**). Immunoblot analysis revealed heterogenous protein expression of typical EV/non-EV and adipose markers across biological replicates of ATEVs, aEVs and bEVs (**Fig. 2G-I**). Notably, while calnexin is typically considered a non-EV marker, calnexin was detected in ATEVs and aEVs (**Fig. 2G, H**), consistent with previous reports of endoplasmic reticulum proteins associated with tissue-derived EVs[32-34]. The presence of adiponectin in early SEC fractions suggests its association with EVs rather than free proteins, as previously reported[11].

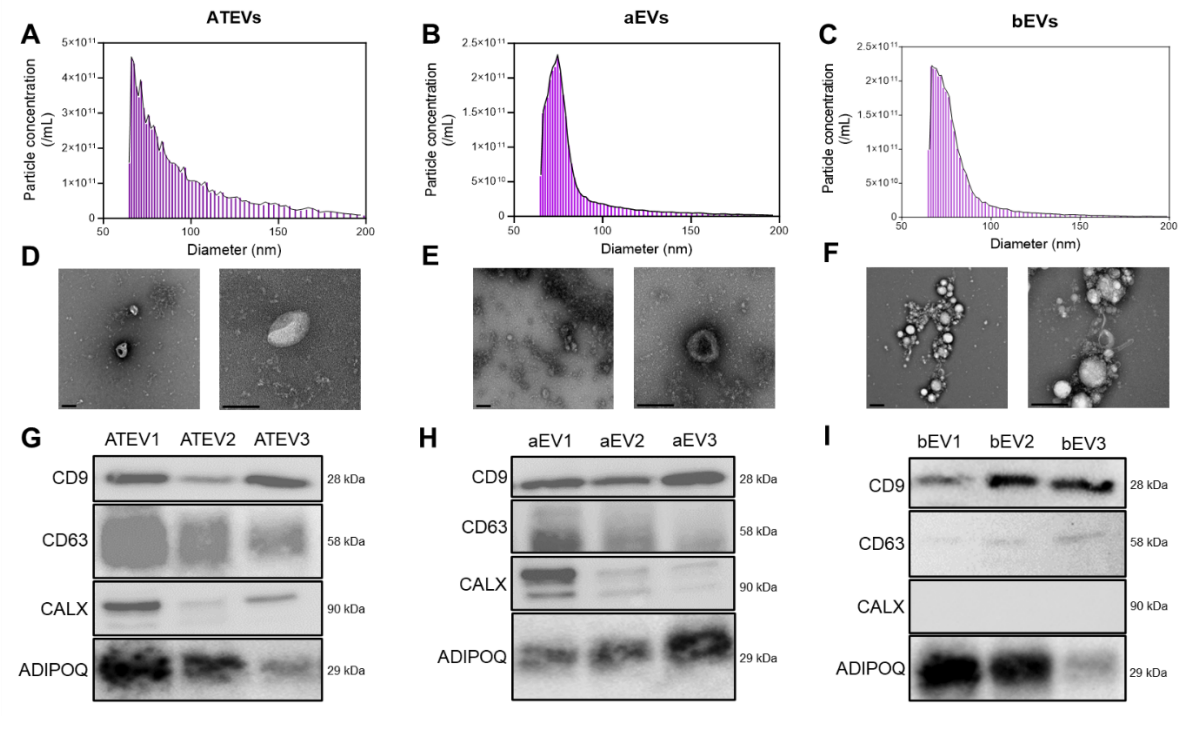

Figure 2. Human adipose EVs exhibited nanoscale size, cup-shaped morphology, classic EV and adipose markers. (A-C) Particle size distribution and concentration analysis via MRPS **(D-F)** TEM images displaying cup-shaped morphology of isolated EVs. **(G-I)** Immunoblotting analysis for EV (CD9 and CD63), non-EV (CALX) and adipocyte markers (ADIPOQ). (n = 3 biological replicates). ATEVs: Adipose Tissue-derived Extracellular Vesicles, aEVs: Mature Adipocyte-derived Extracellular Vesicles. CD9: Cluster of Differentiation 9, CD63: Cluster of Differentiation 63, CALX: Calnexin, ADIPOQ: Adiponectin.

114 **Human ATEVs and aEVs exhibit unique and shared proteomes and biological relevance**
115 **to obesity-associated metabolic and immune processes**

116 Next, we aimed to develop an 'adipose EV signature,' by first performing bulk proteomics
117 (**Fig. 3**) to explore the unique and shared proteomes of adipose tissue EVs (reflecting the
118 complex adipose tissue microenvironment) and mature adipocyte EVs (reflecting the 'purest'
119 adipose reference material). Three-way Venn diagram revealed 548 unique ATEV proteins, 116
120 unique aEV proteins, and 1233 shared proteins (**Fig. 3A**). The overlapping proteins suggest
121 potential functional similarities and shared signaling pathways, while the unique proteins signify
122 specific molecular characteristics associated with each group. We then generated a heat map to
123 visualize the top 50 most abundant proteins in ATEVs and aEVs (**Fig. 3B**). This data set
124 informed our design of single EV immunocapture probes against adipose-enriched candidates
125 (see **Fig. 5**). **Supplementary Table 1** lists the most abundant unique and shared proteins.

126 To investigate canonical biological processes and molecular functions associated with
127 the identified proteins in both ATEVs and aEVs, we performed Gene Ontology (GO) pathway
128 analysis (**Supplementary Fig. 1A,B**). Biological processes identified in our analysis highlighted
129 several significant pathways, including genomic stability and DNA processing and chromatin
130 remodeling. Our study revealed the involvement of ATEVs and aEVs in processes such as pre-
131 replicative complex assembly, regulation of cellular amino acid metabolic processes, cell
132 adhesion, and regulation of transcription from RNA polymerase II promoter in response to
133 hypoxia. Pathways responsible for antigen processing and presentation, cell adhesion, and
134 protein-protein interactions were also identified.

135 KEGG pathway analysis provided further insights into the potential pathobiological
136 relevance of ATEVs and aEVs (**Supplementary Fig. 1C**). Prominent pathways were related to
137 protein processing, quality control and degradation (e.g. proteasome, protein degradation, and
138 endoplasmic reticulum). Additional pathways included neutrophil extracellular trap formation,
139 focal adhesion, metabolic pathways, regulation of actin cytoskeleton, complement and
140 coagulation cascades, leukocyte transendothelial migration, phagosome formation,
141 glycolysis/gluconeogenesis, ECM-receptor interaction, and N-glycan biosynthesis. These
142 pathways imply potential roles of ATEVs and aEVs in processes related to immune responses,
143 cell adhesion, cellular metabolism, cytoskeletal regulation, and intercellular communication.
144 Moreover, pathways associated with cholesterol metabolism, carbon metabolism, fatty acid
145 degradation, platelet activation, endocytosis, antigen processing and presentation, PPAR
146 signaling, and fatty acid metabolism were also identified.

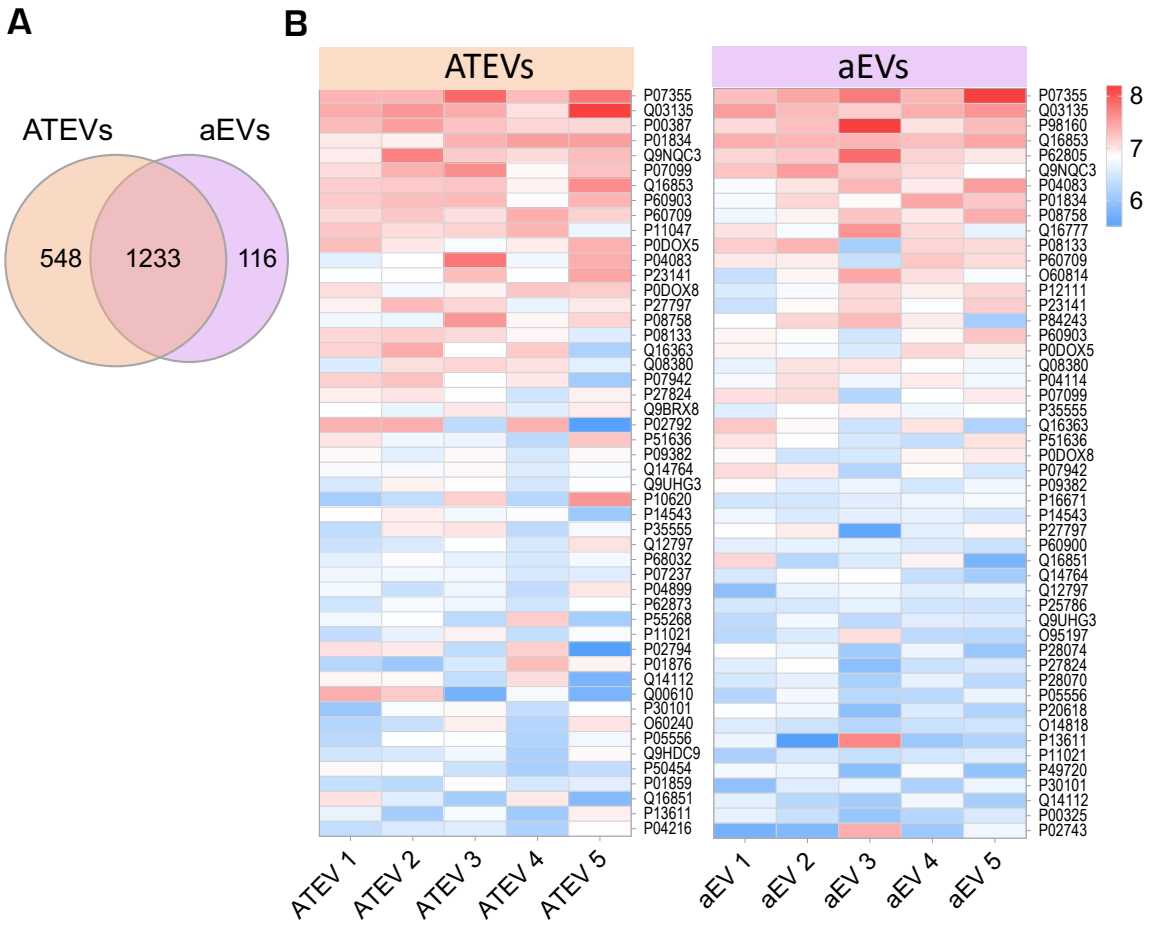

Figure 3. Proteomics analysis of paired human adipose EVs. EVs isolated from paired visceral adipose tissue (ATEVs) and cultured mature adipocytes (aEVs) underwent proteomics analysis. **(A)** Three-way Venn diagram revealed proteins identified in both ATEVs and aEVs (n=1233), with 548 proteins exclusively found in ATEVs and 116 proteins exclusively found in aEVs. **(B)** Heat maps of the top 50 enriched proteins in ATEVs (orange) and aEVs (purple). (n = 3 biological replicates). ATEVs: adipose tissue-derived extracellular vesicles, aEVs: mature adipocyte extracellular vesicles

Multiparametric single EV analysis of human adipose-derived EVs

Orthogonal and complementary single EV methods were utilized to characterize EV size, tetraspanin distribution, EV and adipose protein targets and select adipose mRNA transcripts in paired ATEVs and aEVs from the same individual.

Single ADEV analysis leveraging single-particle interferometric reflectance imaging sensor (SP-IRIS)

161 SP-IRIS[35] with fluorescence was employed to gain insights into the complexity and
162 heterogeneity of tetraspanin distribution across biologically similar but distinct adipose-enriched
163 EV subsets at single EV resolution (**Fig. 4**). Single EVs (sEVs) were immunologically
164 immobilized/captured by surface tetraspanin proteins CD63, CD81, and CD9 printed on a
165 microchip surface. Fluorescently-labelled anti-CD63, anti-CD81 and anti-CD9 antibodies were
166 added for detection. Capture events were counted (mean particle count) and sEVs were sized
167 by light interference (lower limit of detection of 50 nm). SP-IRIS revealed a particle size scatter
168 of 50 nm to 200 nm for both ATEVs and aEVs (data not shown), which was consistent with
169 MRPS size analysis. Quantification of events per capture chip revealed a notable presence of
170 particles, indicating successful ATEV (**Fig. 4A, C**) and aEV (**Fig. 4B, D**) capture. Both ATEVs
171 and aEVs demonstrated the most total capture events with CD63 capture and greater CD63
172 detection from the CD63 capture spot. CD81 capture resulted in similar expression patterns for
173 ATEVs and aEVs while CD9 capture revealed higher CD9 detection for aEVs but not ATEVs
174 (**Fig. 4A, B**).

175 Tetraspanin colocalization analysis revealed distinct patterns among the CD63, CD9,
176 and CD81 capture spots **(Fig. 4C,D; Supplementary Fig. 2)**. CD63 was the most prevalent
177 single-positive tetraspanin detected on both ATEVs and aEVs immobilized on the CD63 capture
178 spot, as visualized by red fluorescence signal (**Fig. 4C,D**). ATEVs and aEVs captured by CD81
179 both had the highest detection for CD9+ single positive EVs, as well as CD63+/CD9+ double
180 positive EVs. CD9 capture differed between ATEVs and aEVs, with greater CD81+ single
181 positive ATEVs and slightly greater CD9+ single positive aEVs. These results indicate that
182 CD63 is the predominant surface marker expressed in both ATEVs and aEVs. Representative
183 images obtained with the SP-IRIS instrument visually confirmed these expression patterns (**Fig.
184 4C,D**). In summary, sEV tetraspanin phenotyping provides valuable insights into the tetraspanin
185 expression profiles and molecular heterogeneity of ATEVs and aEVs.

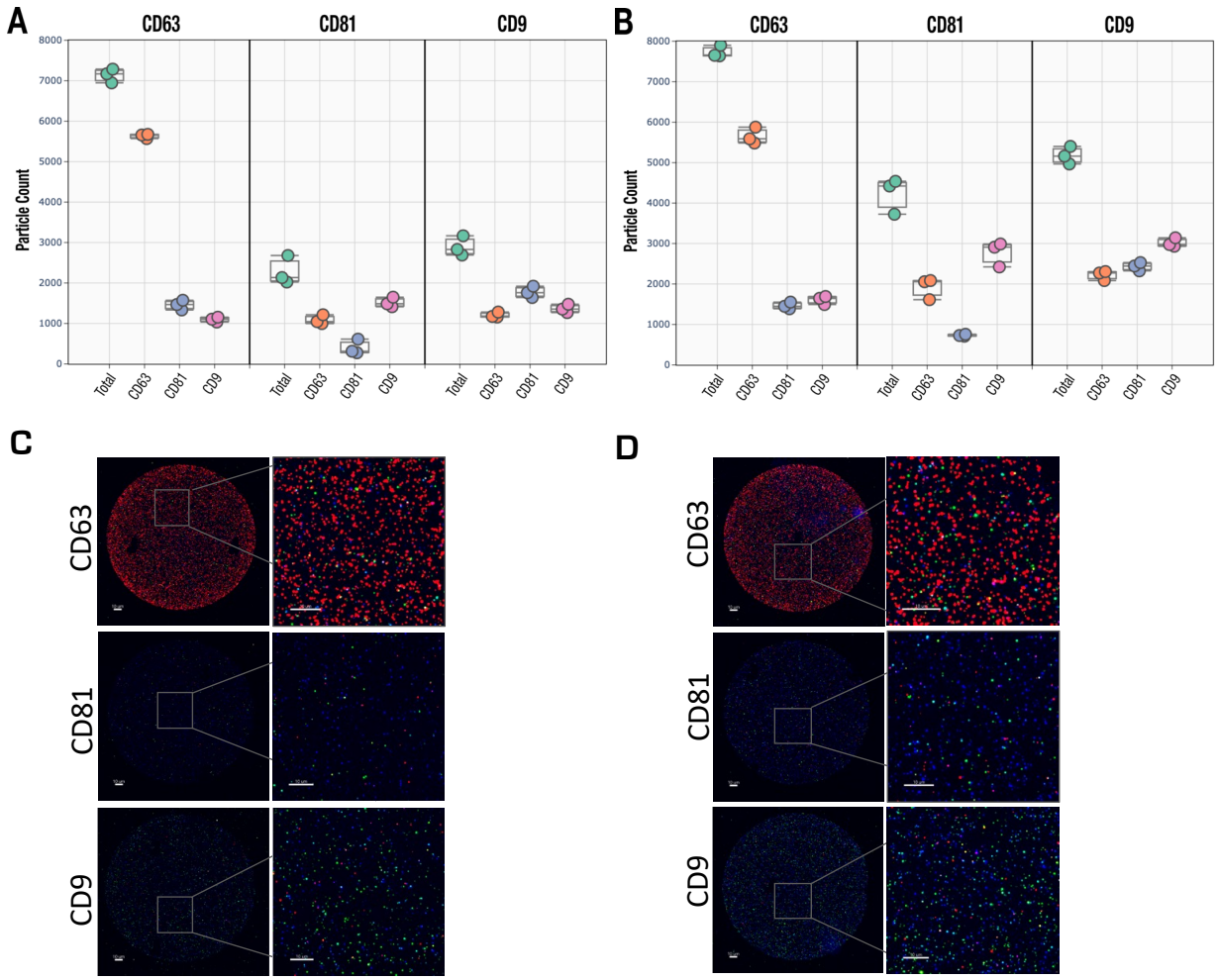

Figure 4. Single ADEV multiplex analysis showed comparable classic EV markers in ATEVs and aEVs. Beeswarm plots showing tetraspanin profiles for ATEVs (**A**) and aEVs (**B**). The x-axis reflects tetraspanin detection antibody and the top label indicates the tetraspanin capture antibody. Both ATEVs and aEVs showed similar but not identical tetraspanin event frequencies (see manuscript text for details; n =3). SP-IRIS representative images per capture spot CD63, CD81, CD9 for ATEVs (**C**) and aEVs (**D**). Scale 10 um. All events were detected above mouse IgG isotype control levels (data not shown).

Total internal reflection fluorescence (TIRF) microscopy allows simultaneous detection of human adipose-derived EV protein and mRNA cargo at single EV resolution

To establish an adipose liquid biopsy for the interrogation of circulating plasma EVs, we next applied our adipose-enriched proteomics candidates to the development of adipose-enriched surface capture targets and molecular beacons for mRNA detection cargo at single EV

200 resolution. After immobilization of EVs using anti-CD63 and CD9 hybridized surface[36], two
201 adipocyte markers (adipocyte plasma membrane protein, APMAP; and perilipin) were selected
202 for detection of adipocyte-specific surface proteins on plasma EVs. Furthermore, we examined
203 the presence of specific mRNA molecules using molecular beacons designed against PPARG
204 and ADIPOQ, which are known to be highly expressed in adipocytes[37-38]. The results of the
205 protein detection revealed the presence of APMAP, perilipin, and CD63 on both single ATEVs
206 and aEVs (**Fig. 5**). Similarly, detection of the molecular beacons confirmed the presence of
207 PPARG and ADIPOQ mRNA within the immobilized vesicles. These results confirm our ability to
208 characterize plasma circulating, adipose-specific single EVs with simultaneous surface protein
209 and mRNA cargo.

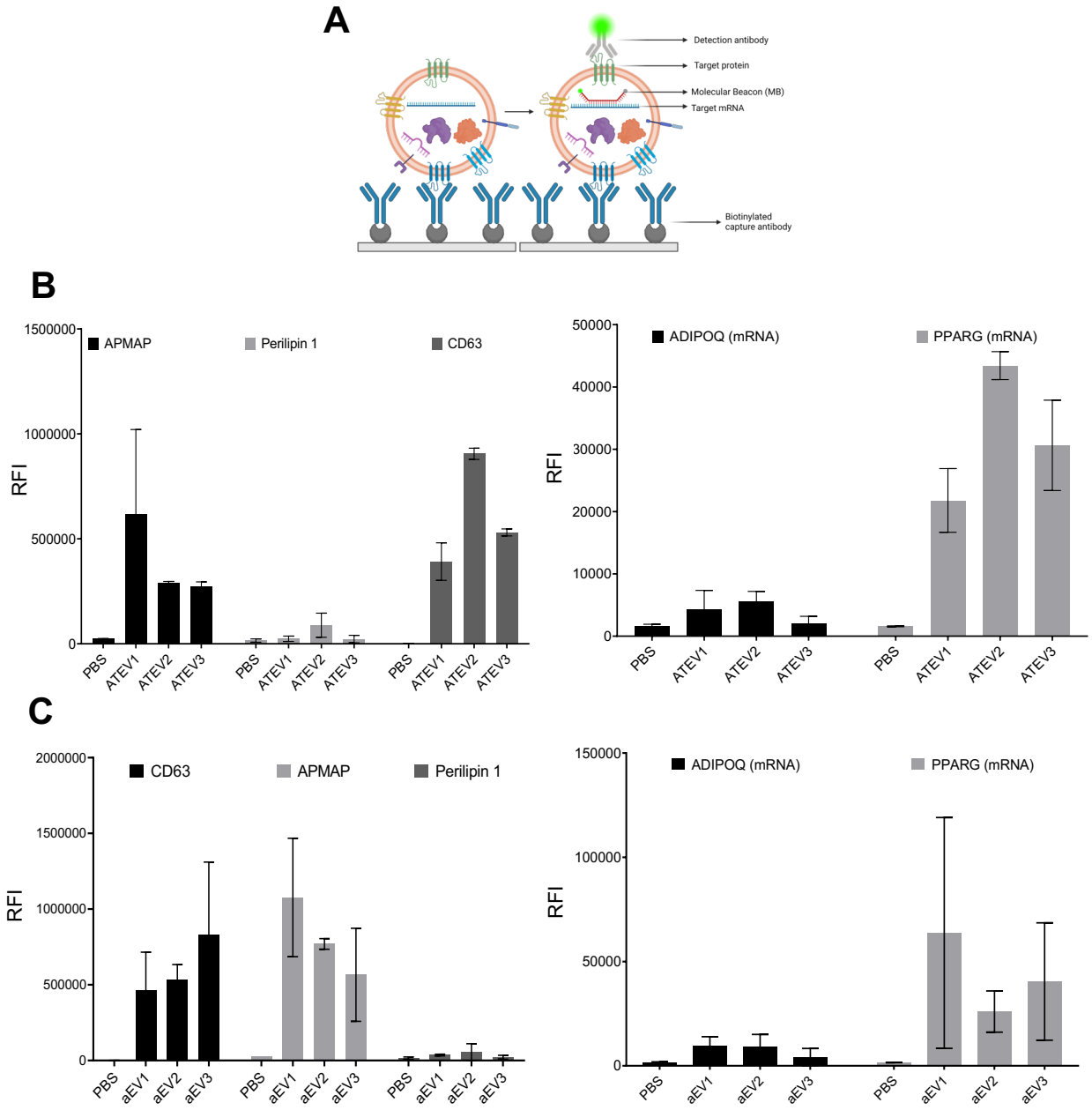

Figure 5. Single ADEV cargo and surface marker analysis defines CD63+/APMAP+/PPARG+ as an adipose-specific EV signature for liquid biopsy development. (A) Schematic showing how TIRF works. **(B)** ATEV and aEV (**C**) TIRF analysis with simultaneous protein (APMAP, perilipin, CD63; left) and mRNA cargo (ADIPOQ, PPARG; right). (n = 3 paired biological replicates). ADIPOQ: Adiponectin, APMAP: adipocyte plasma membrane-associated protein, PPARG: peroxisome proliferator-activated receptor gamma, ADEV: adipose-derived EVs, ATEVs: adipose tissue-derived EVs, aEVs: mature adipocyte derived EVs

219 **Multiparametric single particle analysis of plasma EVs and validation of an adipose liquid**
220 **biopsy**

221 Lastly, to explore the liquid biopsy utility of our adipose-derived EV analysis, we applied
222 two complementary single EV methods to the plasma EVs (bEVs) that corresponded to the
223 matched ATEVs and aEVs from the same individual (**Fig. 1, Fig. 4, Fig. 5**). SP-IRIS analysis
224 was used to explore the tetraspanin distribution of bEVs and unlike the matched ATEV and aEV
225 analyses, CD81 capture, rather than CD63 capture, resulted in the greatest total mean particle
226 count and of CD81+ single positive EVs (**Fig. 6A,B**). Colocalization analysis demonstrated a
227 high percentage of CD63+/CD81+ double-positive bEVs (**Supplementary Fig. 3**). These results
228 underscore the heterogeneity of EV subsets across various biospecimens.

229 TIRF analysis of bEVs (**Fig. 6C,D**) and neat plasma (**Fig. 6E,F**) was employed to
230 validate our ability to capture and characterize adipose-derived EVs in the circulation of bariatric
231 patients. We successfully captured single, plasma-derived EVs that displayed EV (CD63) and
232 adipocyte surface markers (APMAP, perilipin) and contained adipocyte mRNA cargo (ADIPOQ,
233 PPARG). We next sought to evaluate the sensitivity of our sEV assay to detect low-abundant
234 ADEVs in the circulation of bariatric patients by performing TIRF analysis on neat plasma (i.e.
235 without EV isolation) from the same patients. We were again able to capture sEVs that
236 displayed EV (CD63) and adipocyte surface markers (APMAP, perilipin) and contained
237 adipocyte mRNA cargo (ADIPOQ, PPARG).

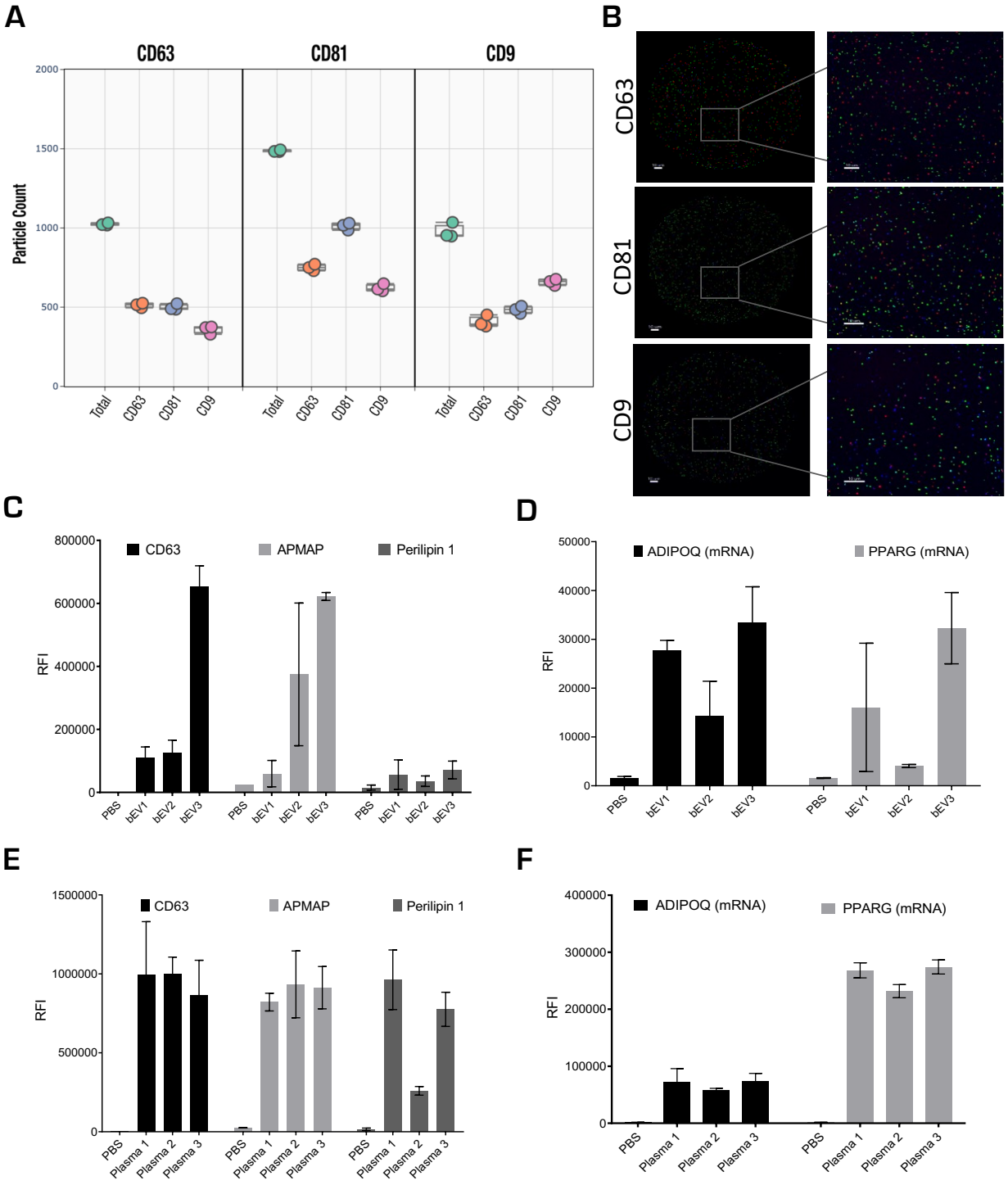

Figure 6. Multiparametric single EV analysis of plasma EVs with simultaneous adipose target protein and mRNA cargo characterization. **(A, B)** SP-IRIS tetraspanin profile characterization and colocalization representative images of bEVs (scale 10um). TIRF analysis on paired SEC-isolated plasma EVs (**C-D**) and neat plasma (**E-F**) from the same individual.

243 Simultaneous adipocyte and EV protein (APMAP, perilipin, CD63; left) and adipocyte mRNA
244 cargo (ADIPOQ, PPARG; right) detection in single EVs from bariatric patient plasma (n = 3
245 paired biological replicates).

246 **Discussion**

247 The dual roles of adipose-derived EVs (ADEVs) as biomarkers and pathogenic
248 conveyors of disease across a diversity of pathologies have recently garnered increased
249 attention[4,25,26,39]. Through the transfer of diverse bioactive cargoes, ADEVs can influence
250 disease mechanisms locally and systemically[26,40-42], particularly at the interface between
251 adipose tissue and systemic metabolic regulation[15]. Despite the growing interest in ADEVs, their
252 full translational potential has been hindered by methodological and biological challenges.
253 Firstly, standardized, reproducible and robust isolation protocols for tissue-derived EVs are
254 lacking[29]. Secondly, most ADEV studies have focused on rodent models[25-27], despite known
255 cross-species differences in adipose biology between rodents and humans[28]. Lastly, cell-
256 specific EV analysis is often technically challenging and also requires a priori knowledge of
257 known cell-specific markers for EV immunocapture[21]. Therefore, innovative approaches for
258 human adipocyte-specific EV analysis are needed to move the translational potential of ADEVs
259 beyond the laboratory and into the clinic.

260 Herein, we present a novel and systematic approach to develop a sensitive and robust
261 human adiposity-associated EV liquid biopsy. By utilizing paired biospecimens from the same
262 individual, we are the first to successfully interrogate paired human adipose EVs from tissue,
263 autologous cells, and plasma at both the bulk and single EV level. While there was expected
264 inter-individual heterogeneity across patients, remarkably, we observed intra-individual
265 similarities in the ADEVs from the same individual, irrespective of EV source (e.g., VAT,
266 cultured adipocytes, plasma). In this proof-of-concept study, we establish the feasibility of
267 analyzing low-abundant ADEVs in the circulation of bariatric patients and thus open new
268 avenues for studying ADEVs across diverse conditions known to be adversely associated with
269 obesity, such as cardiovascular disease[2], cancer[43], autoimmunity[44] and neurodegenerative
270 diseases[6].

271 **Biological insights from adipose-derived extracellular vesicle proteomics**

272 Adipose-derived EVs (such as ATEVs and aEVs) are central players in the growing field
273 of adipose tissue interorgan crosstalk and provide added complexity and scope to the adipose
274 secretome[15,42,45]. To gain insights into the potential novel contributions of EVs to the adipose

275 secretome, we performed bulk proteomics, KEGG and GO enrichment analysis on ATEVs and
276 aEVs. Our results confirm previous studies that EV biology, as reflected by the EV proteins
277 ANXA2[46], ANXA1[47], and CAV1[48], is a prominent aspect of the adipose milieu[15,20,45]. Additionally,
278 while ATEVs and aEVs exhibited shared proteomes, the analysis also revealed distinct proteins
279 between ATEVs and aEVs, reflecting diverse functional domains. Adipocyte EVs were primarily
280 enriched in histone proteins (H2BC26, MACROH2A1)[49], suggesting a more prominent role of
281 aEVs compared to ATEVs in chromatin remodeling and gene regulation. ATEVs were enriched
282 in proteins involved in proteasomal degradation (PSMD12, PSMD3) that have been implicated
283 in several cancers and neurodevelopmental disorders[50-52]. ATEVs were also enriched in the
284 autophagosomal regulator, SACM1L, which interestingly is the only phosphatidylinositol-4-
285 phosphate-specific phosphatase in humans[53,54].

286 A secondary objective of profiling the ATEV and aEV proteomes was to screen for
287 adipose-enriched candidates for subsequent adiposity liquid biopsy analysis from plasma. The
288 concept of liquid biopsy originates from the cancer field and encompasses minimally invasive
289 sampling of biofluids for circulating nanoparticles that reflect a tumor or tissue's molecular
290 signature—thereby obviating the need for tissue acquisition[55]. While early liquid biopsy studies
291 focused on circulating, cell-free tumor DNA or RNA, the discovery of EVs being found in every
292 biofluid studied has expanded the liquid biopsy field to include EVs as versatile and robust liquid
293 biopsy sources[21,56,57]. Toward this end, we leveraged our ADEV proteomics results to select
294 APMAP and perilipinas candidate adipose-enriched proteins for our plasma single EV analysis
295 and adiposity liquid biopsy development (see below). Both proteins are known to be involved in
296 diverse cellular functions, including adipocyte differentiation[58,59], adipogenesis[60,61], and insulin
297 resistance[60,62]. Notably, APMAP is also highly expressed in the brain where it appears to
298 complex with secretases involved in amyloid beta regulation. APMAP is additionally involved in
299 neuronal differentiation, mRNA splicing and the autophagy-lysosomal system[63,64]. In summary,
300 these results highlight the pathobiological relevance and biomarker potential of the human
301 ADEV proteome.

302 **Single ADEV multiplex analysis as a next-generation tool for adiposity liquid biopsy**
303 **development**

304 We leveraged two complementary, next-generation microchip-based platforms to
305 comprehensively phenotype paired human ADEVs from multiple sources at single EV
306 resolution[21]. SP-IRIS[35] and TIRF microscopy have emerged as valuable tools for the
307 visualization, quantification, and characterization of individual EVs[65,66]. SP-IRIS analysis allows

308 tetraspanin phenotyping at the single EV level. While CD9 and CD63 are commonly considered
309 pan-EV markers, it is known that tetraspanin profiles are heterogenous in presence and
310 quantity, depending on EV source, and can offer insights into EV subtypes[35]. In our paired
311 biospecimens, CD63 was the predominant tetraspanin expressed in ATEVs and aEVs but not in
312 plasma EVs from the same individual. These results highlight the molecular heterogeneity of EV
313 subsets from different biospecimens and underscore the need to use multiple EV surface
314 markers for immunocapture and/or characterization[35].

315 We employed TIRF microscopy as an ultrasensitive, high-resolution technique for the
316 simultaneous detection of specific proteins and mRNA molecules within immobilized paired
317 ATEVs, aEVs, bEVs and neat plasma from the same individual[66]. Starting with EVs from the
318 'primary source' (i.e. ATEVs and aEVs), TIRF microscopy defined our adiposity EV signature as
319 CD63+/APMAP+/PPARG+/ADIPOQ^{low}. Next, we technically validated the
320 CD63+/APMAP+/PPARG+/ADIPOQ^{low} adiposity EV signature in bEVs and neat plasma from
321 the same biological replicates. EVs isolated from paired plasma (bEVs), compared to matched
322 ATEVs and aEVs, demonstrated greater variable expression of CD63, APMAP, ADIPOQ and
323 PPARG. Notably, neat (unprocessed) plasma largely maintained the 'primary source' adiposity
324 EV signature with high CD63+/APMAP+/PPARG+/ADIPOQ^{low}. This observation bolsters the
325 utility of neat plasma EVs as suitable for tissue and cell-specific liquid biopsy applications.

326 **Challenges and future direction**

327 Tissue-derived EVs constitute only 0.2% of the total plasma EV pool, underscoring the
328 technical challenges in studying low abundance, tissue-derived and cell-specific EVs. Despite
329 this signal-to-noise challenge, adipose tissue is the most prominent contributor (>82%) of
330 tissue-derived EVs in human plasma[67], allowing us to employ our next generation, ultrasensitive
331 single EV methods to define an adiposity EV signature for liquid biopsy application. In this
332 innovative study, we are the first describe a multiparametric pipeline to characterize bulk and
333 single ADEVs from paired human visceral adipose tissue, autologous mature adipocytes, and
334 plasma. Importantly, this research pioneers the direct detection of an adipose-specific EV
335 signature from bariatric patient unprocessed plasma. Our study paves the way toward an
336 obesity EV liquid biopsy and broadens the therapeutic landscape of novel, human adipose-
337 enriched EV candidates worthy of future translational application.

338

339

340 **Methods**

341 Our study adheres to all applicable ethical regulations. The OSU Institutional Review
342 Board (IRB) approved the study, and all participants provided written informed consent. While
343 the study involved human subjects, they were not prospectively assigned to an intervention to
344 evaluate the effect on health-related biological outcomes or compare diets or treatments. As a
345 result, the study is exempt from registration in Clinical Trials.gov.

346 **Study participants:** VAT biopsies and plasma samples were obtained from patients with
347 obesity (n = 11, average age: 41.6 years old SD: 12.98, BMI: 40.97, SD: 6.00) who underwent
348 elective bariatric surgery at The Ohio State University (OSU) Center for Minimally Invasive
349 Surgery. Clinical data is summarized in **Supplementary Table 2**. Subjects received no
350 compensation for participation.

351 **Adipose tissue dissociation and mature adipocyte culture for EV isolation:** Adipose tissue
352 samples were obtained during bariatric surgery and dissociated within an hour from
353 procurement using collagenase digestion. The resulting cell suspension was centrifuged at 500
354 x g for 10 minutes to separate the mature adipocytes, the stromal vascular fraction (SVF), and
355 the dissociation solution. The mature adipocytes were cultured for 24 hours in Dulbecco's
356 Modified Eagle Medium/Ham's Nutrient Mixture F-12 (DMEM/F12), supplemented with 40%
357 M199 basal medium with Earle's salts and L-glutamine (MCDB201 Media), 2% Fetal Bovine
358 Serum (FBS), 1x Penicillin/Streptomycin, 1 nanomolar (nM) dexamethasone, L-ascorbic acid 2-
359 phosphate (LAAP) 0.1 millimolar (mM), Insulin-Transferrin-Selenium (ITS) MIX 1x, Linoleic acid-
360 Albumin 1x, insulin 5 micrograms per microliter (ug/uL), and Triiodothyronine (T3) 1 nM.

361 **ADEV isolation via tangential flow filtration (TFF):** Adipose tissue dissociation media and
362 mature adipocyte culture media were first filtered through 0.2um filters. Media was subsequently
363 concentrated into 5 ml and diafiltrated using TFF with a 500 kDa filter for purification at a flow
364 rate of 35 ml/min as previously described[68]. After TFF, the retentates were concentrated using
365 centrifugal units (30 kDa MWCO, MilliporeSigma Amicon Ultra Centrifugal Filter Unit, Fisher
366 Scientific) at 4000 × g for 30 min to a final volume of 100uL.

367 **Plasma EV isolation via size exclusion chromatography (SEC):** Whole blood was collected
368 in (ethylenediaminetetraacetic acid) EDTA tubes and centrifuged at 1500 x g, 10min at RT to
369 separate the plasma from blood cells. The plasma was then transferred to a new tube and
370 subjected to two sequential centrifugations at 2,500 x g for 15 min at RT. The resulting platelet-
371 depleted plasma was collected and subjected to EV isolation via SEC using the qEV single EV

372 columns. A total of 8 fractions were collected, and fractions 1-4 were used for EV
373 characterization. Briefly, 150 µL of the platelet-depleted plasma was loaded onto the top of the
374 qEV column, and EVs were separated based on their size and surface properties. The column
375 was eluted with phosphate-buffered saline, and 200 µL fractions were collected. Fractions 1-4
376 were pooled and concentrated using centrifugal filters units (30 kDa MWCO, MilliporeSigma
377 Amicon Ultra Centrifugal Filter Unit, Fisher Scientific) at 4000 × g for 30 min to a final volume of
378 100uL.

379 **Microfluidic resistive pulse sensing (MRPS):** Particle number concentrations and size
380 distributions were measured by microfluidic resistive pulse sensing using the Spectradyne nCS1
381 instrument (Spectradyne, Torrence, CA) equipped with C-400 polydimethylsiloxane cartridges to
382 cover a size range of approximately 65-400nm in vesicle diameters. Data analysis was
383 performed with the nCS1 Data Analyzer (Spectradyne).

384 **Western blotting:** EV samples were lysed in radioimmunoprecipitation assay (RIPA) buffer
385 (Thermo Scientific, Cat# J62524AD) with the addition of Thermo Scientific Pierce Protease and
386 Phosphatase Inhibitor (Thermo Scientific, Cat#A32959) for 15 min on ice. Protein
387 concentrations were quantified using a Micro BCA™ Protein Assay Kit (Thermo Scientific, Cat#
388 23235). Equivalent amounts of sample proteins in Laemmli buffer (With reducing agent, 2-
389 Mercaptoethanol (Sigma-Aldrich, CAT# 8057400005) were electrophoresed on 4-20% Mini-
390 PROTEAN® TGX Stain-Free gels (Bio-rad, Cat#4568096) and then transferred onto a
391 polyvinylidene fluoride (PVDF) membrane (Biorad, Cat#1620177). Membranes were blocked
392 and then probed with primary antibody diluted in TBS-T overnight at 4°C and then with
393 horseradish peroxidase conjugated secondary antibody for 1 hour at RT. Immunoreactivity was
394 determined using enhanced chemiluminescence (ECL) solutions (Biorad, Cat# 1705060) and
395 visualized using a Biorad ChemiDoc™ MP imaging system.

396 **Single-particle interferometric reflectance imaging sensing (SP-IRIS):** Unchained Labs
397 (Boston, MA, USA) silicone chips coated with tetraspanin-specific capture spots (CD63, CD9,
398 and CD81) and a negative control spot (mouse IgG isotype). Chips were incubated for 1 hour at
399 RT with 1 × 10E8 ADEVs and 1x10E7 plasma EVs diluted in a final volume of 60 µL of
400 incubation buffer A at room temperature. After the incubation, chips were washed 3 times for 3
401 min on an orbital plate shaker with wash solution B. The chips were scanned with the SP-IRIS™
402 R200 reader (Unchained labs) by the ExoScanner software (Unchained labs, Boston, MA,
403 USA). The data was analyzed using SP-IRISer software (Unchained labs, Boston, MA, USA).

404 **Transmission electron microscopy:** Two 20-μL droplets of deionized (DI) water and two
405 droplets of UranyLess EM contrast stain (Electron Microscopy Science) were placed on a
406 parafilm surface. Prior to that, TEM grids underwent a 1-minute plasma treatment.
407 Subsequently, 10 μL of ATEVs, aEVs, and bEVs were deposited onto the plasma-treated
408 surface through drop-casting. The samples were allowed to incubate on the TEM surface for 1
409 minute, followed by gentle blotting with filter paper to remove excess liquid. The TEM grids were
410 promptly washed by dipping them into a DI water droplet, followed by blotting with filter paper.
411 This washing step was repeated with another DI water droplet. The same technique was then
412 repeated for the contrast stain, with each incubation lasting 22 seconds. The TEM grids were
413 carefully stored in a grid box overnight to ensure complete drying before imaging. TEM imaging
414 was performed using a Tecnai TF-20 microscope operating at 200kV.

415 **Single EV analysis using Total internal reflection fluorescence microscopy**

416 **Antibody functionalization of the biochip:** In accordance with the methodology delineated in
417 the preceding publication, a biochip featuring a gold-coated substrate was painstakingly
418 prepared and subsequently functionalized using biotin-PEG-SH[36]. The functionalization of the
419 biochip with antibodies entailed a series of specific steps. A uniform working volume of 20 μL
420 was employed in each well to introduce various solutions. To ensure an even distribution of
421 solutions within the wells, all incubation stages were conducted on a shaker. Before the
422 antibody functionalization, a thorough washing of each well was conducted by pipetting DI water
423 ten times. Following this, a solution of NeutrAvidin (NA; Thermo Fisher Scientific) at a
424 concentration of 50 μg/mL, diluted in phosphate-buffered saline (PBS; Thermo Fisher Scientific),
425 was added to each well. This mixture was allowed to incubate at room temperature for 1 hour to
426 bind with the biotin motifs on the gold surface. Excess NeutrAvidin was subsequently removed
427 by pipetting PBS ten times, and this rinsing process was repeated three times.

428 **Introduction of biotinylated capture antibodies:** For the introduction of biotinylated capture
429 antibodies, the antibodies were first biotinylated using the EZ-Link micro Sulfo-NHS-biotinylation
430 kit (Thermo Fisher Scientific). Each antibody was then diluted to a concentration of 10 μg/mL in
431 a 1% (w/v) solution of bovine serum albumin (BSA; Sigma-Aldrich) in PBS. The prepared
432 biotinylated capture antibody mixture was added to each well and allowed to incubate at room
433 temperature for 1 hour. To remove excess protein, the wells were washed by pipetting PBS up
434 and down ten times, with this rinsing process being repeated three times.

435 **Molecular beacons hybridization:** The molecular beacons (MBs) were diluted down to a
436 concentration of 5 μM for each individual MB, using 12.5 × Tris EDTA (TE) buffer (Sigma-
437 Aldrich), which was diluted in deionized (DI) water. This dilution served the dual purpose of
438 stabilizing the MBs and permeabilizing the RNA-encasing membrane. The resulting mixture of
439 MBs was subsequently diluted by a factor of 25 within the biofluid sample, and the biochip was
440 then subjected to a 2-hour incubation period at 37°C, creating an environment devoid of light to
441 facilitate the hybridization of the MBs with the target RNA.

442 **Capture of EVs on biochip surface:** In each well, a solution of BSA in PBS, with a
443 concentration of 3% (w/v), underwent a 1-hour incubation at room temperature. This step aimed
444 to prevent nonspecific EV capture and maintain single-vesicle resolution. Following the removal
445 of BSA, the biofluid samples were then introduced into the wells and allowed to incubate for 2
446 hours at room temperature under dark conditions. PBS was introduced into the wells for a 5-
447 minute incubation period, followed by pipetting PBS up and down ten times to eliminate
448 excessive EVs and unhybridized MBs. This rinsing process was repeated four times within a
449 dimly lit environment.

450 **Detection antibodies targeting membrane proteins:** Initially, a solution of BSA at a
451 concentration of 3% (w/v) in PBS was added to each well and incubated at room temperature
452 for one hour. This step aimed to prevent the nonspecific binding of the fluorophore-conjugated
453 antibodies (detection antibodies). After the BSA solution was removed, a solution containing
454 detection antibodies at a concentration of 1 μg/mL was prepared in 10% (w/v) normal goat
455 serum (NGS; Thermo Fisher Scientific). Subsequently, the wells were subjected to a one-hour
456 incubation at room temperature in a dark setting. To eliminate excess detection antibodies, PBS
457 was added to the wells and allowed to incubate for 5 minutes. Following this, gentle pipetting up
458 and down of the solution was carried out ten times. The rinsing procedure was repeated thrice
459 within a dimly lit environment.

460 **EV proteomics digestion:** EVs were digested using Protifi S-trapTM and the published
461 protocol was adapted to fit the project needs. (1) Briefly, samples were digested in lysis buffer
462 consisting of 10% Sodium Dodecyl Sulfate (SDS) with 100 millimolar (mM) tetraethylammonium
463 bromide (TEAB). Samples were sonicated and then clarified by centrifugation. Protein
464 concentration was determined using NanoDrop A280 (Thermo Fisher Scientific). Disulfide
465 bonds were reduced by addition of dithiothreitol (DTT), final concentration 20 mM, and
466 incubation at 95 ºC for 15 minutes. Free cysteines were alkylated by the addition of
467 iodoacetamide at a final concentration of 40 mM, followed by incubation in the dark for 30

468 minutes at room temperature (RT). Unreacted iodoacetamide was removed by centrifugation,
469 after which the supernatant was collected. Samples were mixed with binding buffer in a 1:6 ratio
470 of sample to buffer volume. The resulting solution was loaded onto a Protifi S-trapTM micro spin
471 column in increments of 300 µL, and centrifuged until all protein was bound to the column. 20
472 µL of digestion buffer was added, containing Trypsin Gold protease, mass spectrometry grade
473 (Promega, ref V528A) in a 1:10 enzyme-to-protein ratio for each sample. Trypsin was
474 resuspended in 50mM triethylammonium bicarbonate (TEAB) at a 1mg/mL concentration for the
475 stock solution (Sigma ref T7408). Samples were kept at 37ºC overnight and eluted with
476 sequential washes of 50 mM TEAB in water, 0.2% formic acid in water, and 0.2% formic acid in
477 50:50 water/acetonitrile. Samples were dried and resuspended in 0.1% formic acid in water for
478 downstream analysis.

479 **LC-MS/MS analysis:** Bottom-up proteomics data were collected on a Bruker Scientific
480 (Billerica, MA) commercial timsTOF Pro instrument coupled to a Bruker Scientific nanoElute LC.
481 For each sample, 200 ng was loaded. Samples were run in data-dependent acquisition (DDA)
482 mode, using parallel accumulation-serial fragmentation (PASEF). The LC column was 25 cm
483 long with 1.7 µm C18 particles (IonOpticks), and samples were run at a rate of 0.401 µL/min,
484 using a linear reverse phase 120-minute gradient with a starting concentration of 2.0%
485 acetonitrile (ACN) with 0.1% formic acid (FA) and ending concentration of 80.0% ACN with
486 0.1% FA over a period of 110 minutes, with a 10-minute ending hold. The equilibration time was
487 estimated at 3.60 minutes. For MS/MS analysis, the mass range was set as 100 to 1700 m/z,
488 with 10 MS/MS scans, dynamic exclusion time of 0.4 min, and collision-induced dissociation
489 (CID) energy starting at 20.00 eV and ending at 59.00 eV.

490 **Proteomics data processing and analysis:** TimsTOF PASEF datasets were processed using
491 FragPipe (v. 19.1) in conjunction with the MS/MS search engine MSFragger (v. 3.7) and
492 IonQuant (v. 1.8.10). The Uniport human reviewed database was downloaded and used as the
493 input fasta file for spectral mapping. Common contaminants and decoys were added using
494 FragPipe software. The fraction of decoys was set to 50% and was generated by reversing
495 sequences from the target database. This target-decoy search was used to control the false
496 discovery rate (FDR). (https://doi.org/10.48550/arXiv.1501.00537) The precursor mass
497 tolerance was 20 ppm, and the enzyme was set to trypsin with 2 missed cleavages. Peptide
498 length was set to 7 – 50, and peptide mass range was 500 – 5,000. Variable modifications were
499 set to include methionine oxidation (+15.9949) and N-terminal acetylation (+42.0106).
500 Carbamidomethylation on cysteine residues from iodoacetamide treatment (+57.021464) was

set as a fixed modification. The number of variable modifications on a given peptide was set to 3. Percolator was used for peptide-spectrum match (PSM) validation, and MS1 quantification was run using match between runs (MBR) with an FDR of 0.01. Intensity was normalized across runs, using a log-ratio approach where the run with the highest number of ions is used as a reference. Peptide-protein uniqueness was set to unique + razor, where unique peptide refers to the number of PSMs that only map to the given protein, and razor refers to the total number of PSMs that in support of a given protein.

FragPipe results were exported as TSV (tab separated value) files, compatible with Excel for downstream processing. For identified proteins, precursor/MS1 intensity values were used as quantitative markers of protein expression. Intensity is defined by IonQuant software as the summed volume of the 0, +1 and +2 isotopes, where the volume is from ion mobility and retention time information. Missing values were replaced with an appropriate low number (5000). For individual protein identifications, values that were > 50% missing from either ATEV or aEV groups were removed. Values that were not consistent (i.e., sometimes present, sometimes missing) across a single group (ATEV or aEV) were also removed. The data were log base 10 transformed and quantile normalized. A two-sided t test was used to compare ATEVs to aEVs. P-values were FDR-corrected using the Benjamini-Hochberg method. A one-sided t-test was used to look at the ratios of donor-matched aEV. FDR of 0.05 was considered significant.

Proteome FragPipe outputs were further processed using the DAVID (Database for Annotation, Visualization, and Integrated Discovery) bioinformatics tool[69,70].The GO (Gene Ontology) pathway and KEGG (Kyoto Encyclopedia of Genes and Genomes) pathway analyses were conducted. The DAVID tool allowed us to select the statistical analysis method, and we opted to use the FDR as a threshold for identifying significant pathway enrichments.

Data availability

All data generated or analyzed during this study are included in this manuscript and its supplementary information file. Further inquiries can be directed to the corresponding author.

Author contributions

P.L.P., W.H., E.R., S.M.M, conceptualization.

E.R., S.M.M. study design and funding acquisition.

P.L.P., D.S., J.G., K.T.N., B.L.B., J.K. S.N., S.A.B., B.J.N., V.W., W.H. investigation and performed research.

P.L.P., J.G., K.T.N., J.K. organization and data analysis.

P.L.P., S.M.M completed the original draft of the manuscript.

E.R., S.M.M. data interpretation, revision, and correction of the manuscript. All authors approved the final version of the manuscript.

Competing interests

The authors declare no competing interests.

Additional information

Correspondence and requests for materials should be addressed to Senior Corresponding author.

Acknowledgements

We would like to thank William Ray for his illustrative media expertise in designing the figures for this project. We also thank Ms. Mary Shows for editorial and proofreading assistance. Drs. Kristy Townsend and Kristin Stanford provided technical input for adipose tissue processing. SMM was supported by intramural funding from the Abigail Wexner Research Institute at Nationwide Children's Hospital and NINDS (5K12NS098482-05). ER was supported by National Institutes of Health (NIH) grants UG3/UH3TR002884 and U18TR003807. The content is solely the responsibility of the authors and does not necessarily represent the official views of the National Institutes of Health.

References

1 Seidell, J. C. & Halberstadt, J. The global burden of obesity and the challenges of prevention. *Ann Nutr Metab* **66 Suppl 2**, 7-12, doi:10.1159/000375143 (2015).

2 Powell-Wiley, T. M. *et al.* Obesity and Cardiovascular Disease: A Scientific Statement From the American Heart Association. *Circulation* **143**, e984-e1010, doi:10.1161/CIR.0000000000000973 (2021).

3 Avgerinos, K. I., Spyrou, N., Mantzoros, C. S. & Dalamaga, M. Obesity and cancer risk: Emerging biological mechanisms and perspectives. *Metabolism* **92**, 121-135, doi:10.1016/j.metabol.2018.11.001 (2019).

4 Picone, P., Di Carlo, M. & Nuzzo, D. Obesity and Alzheimer's disease: Molecular bases. *Eur J Neurosci* **52**, 3944-3950, doi:10.1111/ejn.14758 (2020).

5 Brenton, J. N. *et al.* Body mass index trajectories in pediatric multiple sclerosis. *Dev Med Child Neurol* **61**, 1289-1294, doi:10.1111/dmcn.14233 (2019).

6 Parimisetty, A. *et al.* Secret talk between adipose tissue and central nervous system via secreted factors-an emerging frontier in the neurodegenerative research. *J Neuroinflammation* **13**, 67, doi:10.1186/s12974-016-0530-x (2016).

7 Kershaw, E. E. & Flier, J. S. Adipose tissue as an endocrine organ. *J Clin Endocrinol Metab* **89**, 2548-2556, doi:10.1210/jc.2004-0395 (2004).

8 Longo, M. *et al.* Adipose Tissue Dysfunction as Determinant of Obesity-Associated Metabolic Complications. *Int J Mol Sci* **20**, doi:10.3390/ijms20092358 (2019).

9 Goossens, G. H. & Blaak, E. E. Adipose tissue dysfunction and impaired metabolic health in human obesity: a matter of oxygen? *Front Endocrinol (Lausanne)* **6**, 55, doi:10.3389/fendo.2015.00055 (2015).

10 Isaac, R., Reis, F. C. G., Ying, W. & Olefsky, J. M. Exosomes as mediators of intercellular crosstalk in metabolism. *Cell Metab* **33**, 1744-1762, doi:10.1016/j.cmet.2021.08.006 (2021).

11 Kranendonk, M. E. *et al.* Human adipocyte extracellular vesicles in reciprocal signaling between adipocytes and macrophages. *Obesity (Silver Spring)* **22**, 1296-1308, doi:10.1002/oby.20679 (2014).

12 Kalluri, R. & LeBleu, V. S. The biology, function, and biomedical applications of exosomes. *Science* **367**, doi:10.1126/science.aau6977 (2020).

13 Kumar, V., Kiran, S., Kumar, S. & Singh, U. P. Extracellular vesicles in obesity and its associated inflammation. *Int Rev Immunol* **41**, 30-44, doi:10.1080/08830185.2021.1964497 (2022).

14 Kwan, H. Y., Chen, M., Xu, K. & Chen, B. The impact of obesity on adipocyte-derived extracellular vesicles. *Cell Mol Life Sci* **78**, 7275-7288, doi:10.1007/s00018-021-03973-w (2021).

15 Bond, S. T., Calkin, A. C. & Drew, B. G. Adipose-Derived Extracellular Vesicles: Systemic Messengers and Metabolic Regulators in Health and Disease. *Front Physiol* **13**, 837001, doi:10.3389/fphys.2022.837001 (2022).

16 van Niel, G., D'Angelo, G. & Raposo, G. Shedding light on the cell biology of extracellular vesicles. *Nat Rev Mol Cell Biol* **19**, 213-228, doi:10.1038/nrm.2017.125 (2018).

17 La Torre, M. E. *et al.* Extracellular Vesicles Cargo in Modulating Microglia Functional Responses. *Biology (Basel)* **11**, doi:10.3390/biology11101426 (2022).

18 Tkach, M. & Thery, C. Communication by Extracellular Vesicles: Where We Are and Where We Need to Go. *Cell* **164**, 1226-1232, doi:10.1016/j.cell.2016.01.043 (2016).

19 Yang, E. *et al.* Exosome-mediated metabolic reprogramming: the emerging role in tumor microenvironment remodeling and its influence on cancer progression. *Signal Transduct Target Ther* **5**, 242, doi:10.1038/s41392-020-00359-5 (2020).

20 Zhao, R., Zhao, T., He, Z., Cai, R. & Pang, W. Composition, isolation, identification and function of adipose tissue-derived exosomes. *Adipocyte* **10**, 587-604, doi:10.1080/21623945.2021.1983242 (2021).
21 Shami-Shah, A., Travis, B. & Walt, D. R. Advances in extracellular vesicle isolation methods: a path towards cell-type specific EV isolation. *Extracell Vesicles Circ Nucleic Acids* **4**, 447-460, doi:10.20517/evcna.2023.14

(2023).
22 Crewe, C. The challenges of interrogating adipose tissue extracellular vesicle functions in physiology. *Commun Biol* **5**, 581, doi:10.1038/s42003-022-03511-9 (2022).
23 Akbar, N., Pinnick, K. E., Paget, D. & Choudhury, R. P. Isolation and Characterization of Human Adipocyte-Derived Extracellular Vesicles using Filtration and Ultracentrifugation. *J Vis Exp*, doi:10.3791/61979 (2021).
24 Connolly, K. D. *et al.* Evidence for Adipocyte-Derived Extracellular Vesicles in the Human Circulation. *Endocrinology* **159**, 3259-3267, doi:10.1210/en.2018-00266 (2018).
25 Kulaj, K. *et al.* Adipocyte-derived extracellular vesicles increase insulin secretion through transport of insulinotropic protein cargo. *Nat Commun* **14**, 709, doi:10.1038/s41467-023-36148-1 (2023).
26 Gesmundo, I. *et al.* Adipocyte-derived extracellular vesicles regulate survival and function of pancreatic beta cells. *JCI Insight* **6**, doi:10.1172/jci.insight.141962 (2021).
27 Durcin, M. *et al.* Characterisation of adipocyte-derived extracellular vesicle subtypes identifies distinct protein and lipid signatures for large and small extracellular vesicles. *J Extracell Vesicles* **6**, 1305677, doi:10.1080/20013078.2017.1305677 (2017).
28 Borgeson, E., Boucher, J. & Hagberg, C. E. Of mice and men: Pinpointing species differences in adipose tissue biology. *Front Cell Dev Biol* **10**, 1003118, doi:10.3389/fcell.2022.1003118 (2022).
29 Vella, L. J. *et al.* A rigorous method to enrich for exosomes from brain tissue. *J Extracell Vesicles* **6**, 1348885, doi:10.1080/20013078.2017.1348885 (2017).
30 Freshney, R. *Culture of animal cells: a manual of basic technique and specialized applications*. 6th edn, (Wiley-Blackwell, 2010).
31 Hearnden, R., Sandhar, B., Vyas, V. & Longhi, M. P. Isolation of stromal vascular fraction cell suspensions from mouse and human adipose tissues for downstream applications. *STAR Protoc* **2**, 100422, doi:10.1016/j.xpro.2021.100422 (2021).
32 Cianciaruso, C. *et al.* Molecular Profiling and Functional Analysis of Macrophage-Derived Tumor Extracellular Vesicles. *Cell Rep* **27**, 3062-3080 e3011, doi:10.1016/j.celrep.2019.05.008 (2019).
33 Cianciaruso, C. *et al.* Primary Human and Rat beta-Cells Release the Intracellular Autoantigens GAD65, IA-2, and Proinsulin in Exosomes Together With Cytokine-Induced Enhancers of Immunity. *Diabetes* **66**, 460-473, doi:10.2337/db16-0671 (2017).
34 Kowal, J. *et al.* Proteomic comparison defines novel markers to characterize heterogeneous populations of extracellular vesicle subtypes. *Proc Natl Acad Sci U S A* **113**, E968-977, doi:10.1073/pnas.1521230113 (2016).
35 Breitwieser, K. *et al.* Detailed Characterization of Small Extracellular Vesicles from Different Cell Types Based on Tetraspanin Composition by ExoView R100 Platform. *Int J Mol Sci* **23**, doi:10.3390/ijms23158544 (2022).
36 Nguyen, L. T. H. *et al.* An immunogold single extracellular vesicular RNA and protein ((Au) SERP) biochip to predict responses to immunotherapy in non-small cell lung cancer patients. *J Extracell Vesicles* **11**, e12258, doi:10.1002/jev2.12258 (2022).
37 Ma, X., Wang, D., Zhao, W. & Xu, L. Deciphering the Roles of PPARgamma in Adipocytes via Dynamic Change of Transcription Complex. *Front Endocrinol (Lausanne)* **9**, 473, doi:10.3389/fendo.2018.00473 (2018).

38 Kern, P. A., Di Gregorio, G. B., Lu, T., Rassouli, N. & Ranganathan, G. Adiponectin expression from human adipose tissue: relation to obesity, insulin resistance, and tumor necrosis factor-alpha expression. *Diabetes* **52**, 1779-1785, doi:10.2337/diabetes.52.7.1779 (2003).
39 Garcia-Contreras, M. & Thakor, A. S. Human adipose tissue-derived mesenchymal stem cells and their extracellular vesicles modulate lipopolysaccharide activated human microglia. *Cell Death Discov* **7**, 98, doi:10.1038/s41420-021-00471-7 (2021).
40 Blandin, A. *et al.* Lipidomic analysis of adipose-derived extracellular vesicles reveals specific EV lipid sorting informative of the obesity metabolic state. *Cell Rep* **42**, 112169, doi:10.1016/j.celrep.2023.112169 (2023).
41 Niu, Q. *et al.* Adipose-derived mesenchymal stem cell-secreted extracellular vesicles alleviate non-alcoholic fatty liver disease via delivering miR-223-3p. *Adipocyte* **11**, 572-587, doi:10.1080/21623945.2022.2098583 (2022).
42 Thomou, T. *et al.* Adipose-derived circulating miRNAs regulate gene expression in other tissues. *Nature* **542**, 450-455, doi:10.1038/nature21365 (2017).
43 Pati, S., Irfan, W., Jameel, A., Ahmed, S. & Shahid, R. K. Obesity and Cancer: A Current Overview of Epidemiology, Pathogenesis, Outcomes, and Management. *Cancers (Basel)* **15**, doi:10.3390/cancers15020485 (2023).
44 Kwiat, V. R., Reis, G., Valera, I. C., Parvatiyar, K. & Parvatiyar, M. S. Autoimmunity as a sequela to obesity and systemic inflammation. *Front Physiol* **13**, 887702, doi:10.3389/fphys.2022.887702 (2022).
45 Crewe, C. & Scherer, P. E. Intercellular and interorgan crosstalk through adipocyte extracellular vesicles. *Rev Endocr Metab Disord* **23**, 61-69, doi:10.1007/s11154-020-09625-x (2022).
46 Hagiwara, K., Katsuda, T., Gailhouste, L., Kosaka, N. & Ochiya, T. Commitment of Annexin A2 in recruitment of microRNAs into extracellular vesicles. *FEBS Lett* **589**, 4071-4078, doi:10.1016/j.febslet.2015.11.036 (2015).
47 Jeppesen, D. K. *et al.* Reassessment of Exosome Composition. *Cell* **177**, 428-445 e418, doi:10.1016/j.cell.2019.02.029 (2019).
48 Crewe, C. *et al.* An Endothelial-to-Adipocyte Extracellular Vesicle Axis Governed by Metabolic State. *Cell* **175**, 695-708 e613, doi:10.1016/j.cell.2018.09.005 (2018).
49 Singh, R., Bassett, E., Chakravarti, A. & Parthun, M. R. Replication-dependent histone isoforms: a new source of complexity in chromatin structure and function. *Nucleic Acids Res* **46**, 8665-8678, doi:10.1093/nar/gky768 (2018).
50 Fararjeh, A. S. *et al.* Proteasome 26S Subunit, non-ATPase 3 (PSMD3) Regulates Breast Cancer by Stabilizing HER2 from Degradation. *Cancers (Basel)* **11**, doi:10.3390/cancers11040527 (2019).
51 Del Valle, L. *et al.* Insulin-like growth factor I receptor activity in human medulloblastomas. *Clin Cancer Res* **8**, 1822-1830 (2002).
52 Ma, J., Zhou, W., Yuan, Y., Wang, B. & Meng, X. PSMD12 interacts with CDKN3 and facilitates pancreatic cancer progression. *Cancer Gene Ther* **30**, 1072-1083, doi:10.1038/s41417-023-00609-y (2023).
53 Liu, K., Kong, L., Graham, D. B., Carey, K. L. & Xavier, R. J. SAC1 regulates autophagosomal phosphatidylinositol-4-phosphate for xenophagy-directed bacterial clearance. *Cell Rep* **36**, 109434, doi:10.1016/j.celrep.2021.109434 (2021).
54 Zhang, H. *et al.* PtdIns4P restriction by hydrolase SAC1 decides specific fusion of autophagosomes with lysosomes. *Autophagy* **17**, 1907-1917, doi:10.1080/15548627.2020.1796321 (2021).
55 Connolly, I. D., Li, Y., Gephart, M. H. & Nagpal, S. The "Liquid Biopsy": the Role of Circulating DNA and RNA in Central Nervous System Tumors. *Curr Neurol Neurosci Rep* **16**, 25, doi:10.1007/s11910-016-0629-6 (2016).

56 Yu, D. *et al.* Exosomes as a new frontier of cancer liquid biopsy. *Mol Cancer* **21**, 56, doi:10.1186/s12943-022-01509-9 (2022).
57 S, E. L. A., Mager, I., Breakefield, X. O. & Wood, M. J. Extracellular vesicles: biology and emerging therapeutic opportunities. *Nat Rev Drug Discov* **12**, 347-357, doi:10.1038/nrd3978 (2013).
58 Albrektsen, T., Richter, H. E., Clausen, J. T. & Fleckner, J. Identification of a novel integral plasma membrane protein induced during adipocyte differentiation. *Biochem J* **359**, 393-402, doi:10.1042/0264-6021:3590393 (2001).
59 Ambele, M. A., Dessels, C., Durandt, C. & Pepper, M. S. Genome-wide analysis of gene expression during adipogenesis in human adipose-derived stromal cells reveals novel patterns of gene expression during adipocyte differentiation. *Stem Cell Res* **16**, 725-734, doi:10.1016/j.scr.2016.04.011 (2016).
60 Ma, Y. *et al.* Identification of a Novel Function of Adipocyte Plasma Membrane-Associated Protein (APMAP) in Gestational Diabetes Mellitus by Proteomic Analysis of Omental Adipose Tissue. *J Proteome Res* **15**, 628-637, doi:10.1021/acs.jproteome.5b01030 (2016).
61 Konige, M., Wang, H. & Sztalryd, C. Role of adipose specific lipid droplet proteins in maintaining whole body energy homeostasis. *Biochim Biophys Acta* **1842**, 393-401, doi:10.1016/j.bbadis.2013.05.007 (2014).
62 Bialesova, L. *et al.* Epigenetic Regulation of PLIN 1 in Obese Women and its Relation to Lipolysis. *Sci Rep* **7**, 10152, doi:10.1038/s41598-017-09232-y (2017).
63 Gerber, H. *et al.* The APMAP interactome reveals new modulators of APP processing and beta-amyloid production that are altered in Alzheimer's disease. *Acta Neuropathol Commun* **7**, 13, doi:10.1186/s40478-019-0660-3 (2019).
64 Zhang, F. *et al.* Clusterin facilitates stress-induced lipidation of LC3 and autophagosome biogenesis to enhance cancer cell survival. *Nat Commun* **5**, 5775, doi:10.1038/ncomms6775 (2014).
65 Arab, T. *et al.* Characterization of extracellular vesicles and synthetic nanoparticles with four orthogonal single-particle analysis platforms. *J Extracell Vesicles* **10**, e12079, doi:10.1002/jev2.12079 (2021).
66 Nguyen, L. T. H. *et al.* An immunogold single extracellular vesicular RNA and protein (AuSERP) biochip to predict responses to immunotherapy in non-small cell lung cancer patients. *Journal of Extracellular Vesicles* **11**, e12258, doi:https://doi.org/10.1002/jev2.12258 (2022).
67 Li, Y. *et al.* EV-origin: Enumerating the tissue-cellular origin of circulating extracellular vesicles using exLR profile. *Comput Struct Biotechnol J* **18**, 2851-2859, doi:10.1016/j.csbj.2020.10.002 (2020).
68 Zhang, J. *et al.* Immunomagnetic sequential ultrafiltration (iSUF) platform for enrichment and purification of extracellular vesicles from biofluids. *Sci Rep* **11**, 8034, doi:10.1038/s41598-021-86910-y (2021).
69 Sherman, B. T. *et al.* DAVID: a web server for functional enrichment analysis and functional annotation of gene lists (2021 update). *Nucleic Acids Res* **50**, W216-W221, doi:10.1093/nar/gkac194 (2022).
70 Huang da, W., Sherman, B. T. & Lempicki, R. A. Systematic and integrative analysis of large gene lists using DAVID bioinformatics resources. *Nat Protoc* **4**, 44-57, doi:10.1038/nprot.2008.211 (2009).